

SCA2003-29: IMPROVEMENT OF FLUID DISTRIBUTION DESCRIPTION DURING FLOODS BY COMBINED USE OF X-RAY CT SCAN AND CONTINUOUS LOCAL RESISTIVITY MEASUREMENTS

Claudine Durand, IFP

This paper was prepared for presentation at the International Symposium of the Society of Core Analysts held in Pau, France, 21-24 September 2003

ABSTRACT

Continuous local resistivity measurements along a plug during drainage-imbibition in a steady state procedure are combined with observations by CT scan during the “plateaux”. This improves the consistency of the description of the experiment, and thus the quality of the parameters that can be drawn from these experiments, and which may be of paramount importance in the log interpretation. Examples are given on Fontainebleau sandstones.

INTRODUCTION

The economical weight of saturation evaluation in oil or gas prospecting is such that the proper choice of the log interpretation models and their calibration are crucial. Resistivity measurements of saturated or unsaturated rock samples have been performed in laboratories for years [1] in order to provide calibration data for log interpretation. These measurements have to be representative, thus exempt of artefacts related to sampling and experimental conditions. Sampling is the first problem to solve: the natural trend of the petrophysicist to chose a “homogeneous” sample is driven both by aesthetic and practical considerations, but also by the easiness of further interpretation. It may however be contradicted by hidden or unavoidable visible heterogeneities. CT scanners [2-4] are more and more widely used to check the homogeneity of the samples before experiment.

Electrical measurements are however rather delicate, and many recommendations have already been put forward by many authors, and the SCA, to prevent inadequate interpretation [5-11]. Operating conditions may be first causes of non linear RI curves. Lyle and Mills [12] have drawn attention on the influence of non uniform core saturation in samples otherwise homogeneous : n is systematically calculated higher than the actual value when operating in a two-electrode system. This non uniformity is purely numerical and geometrical, and does not make any hypothesis on the way of establishing the saturation nor on the capillary equilibrium. Sprunt et al, [13] have shown that, even when operating in a four-electrode system, with samples desaturated by steps using a porous plate, and letting time enough to equilibrate, non uniform saturation may be found, and lead to curved RI-Sw crossplots.

Centrifuge has several times been pointed out as providing non uniform saturation, even with an equilibration time [14]. Porous plate is supposed to give better homogeneity, but no controls have been shown, as far as we know. Continuous injection has been widely

used and checked [15-18], and the possible artefacts taken into account. Other techniques assume on the basis of simulations that the whole sample is analysed, and that no end effect take place, or propose some correcting simulations. However, knowledge of the actual fluid distribution is the better check.

Therefore, In Situ Saturation Monitoring (ISSM) is more and more used [19-21] to follow the saturation of fluids in flow experiments. Use of these measurements assume that the sections are representative of the whole volume in which the fluids flow. Use of CT-scanners, which provides stacks of reconstructed bidimensional “slices” that may be reconstructed as 3D, appears as a good tool to check the distribution of fluids, thus to quantify the zones where they are really homogeneous.

Continuous recording of resistivity measurements along the sample can be performed with very short acquisition periods. They show the homogeneity/heterogeneity of the measurements and can be related to the distribution of porosity described by the CT-scan images. They indicate the kinetics of the establishment of plateaux, and help to take significant pictures by CT-scan. Measurement of the formation factor using different fluid salinities can thus be monitored. Resistivity indices as a function of local saturation can be calculated, and compared with the usual values drawn from the volume balance and the electrical measurements over the whole sample. Combination of all information offers the opportunity of managing the experiment, discarding the unavoidable artefacts, thus interpreting the measurements in a way consistent with their further use.

The paper describes the experimental equipment, and presents preliminary results obtained on model sandstones. Additional data on carbonates and further interpretation will be given in another paper [22].

PROCEDURES

Electrical and Volume Measurements

The experimental setting is shown on Figure 1. The cell containing the sample is positioned in the CT-scanner, and is not displaced during the experiment. Flow experiments are run in a cell made of light aluminium alloy and equipped with a sleeve (Ergotech) bearing six potential electrodes spaced 1.25 cm apart on each side along the sleeve and sample (Figure 2). The confining pressure is maintained by nitrogen at about 30 bars. The equipment allows measurements in 2- or 4-electrode mode, with the two current electrodes at each end of the plug, and the potential electrodes along the sample (Figure 2). No ceramic nor porous plate is used. Water and oil are injected simultaneously for the steady state procedure, oil only or water only at the end of the drainage/imbibition steps, in order to observe the effects of a “bump” procedure frequently used in practical experiments. The fluid circuit is closed, thus allowing a perfect volume balance of the fluids. The fluid levels are read by eye, and corrected for the volume of the plunging tubes and the pressure sensors, thus providing an average saturation measurement.

Electrical measurements are performed with a Hewlett-Packard impedance meter 4263B. The conditions are 1V, 1kHz. The phase angle is negligible at this frequency. Resistance measurements are acquired on a personal computer every 1 to 15 minutes on each “slice” (i.e. interval between the potential electrodes) of sample, both in 2- and in 4-electrodes setting, without any manipulation of the sample during the whole experiment. Temperature, inlet pressure and differential outlet-inlet pressure are monitored at the same rate as the resistances. This allows temperature correction for the resistances.

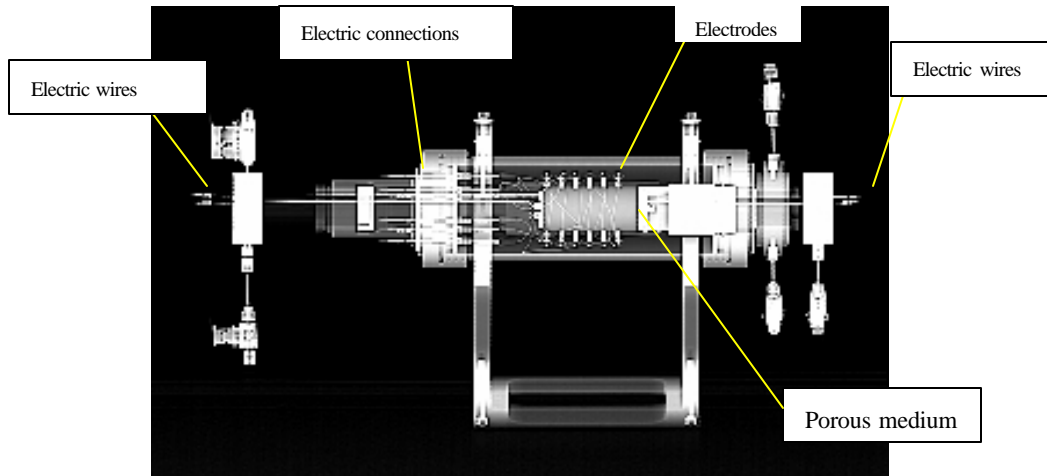


Figure 1: Radiography of the cell

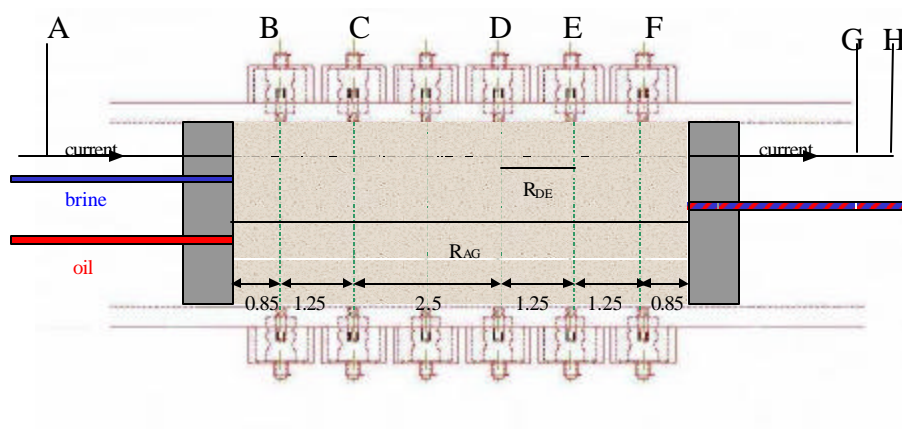


Figure 2: Setting of the sample in the sleeve, with the current electrodes A and H, and the potential electrodes, B to G. A and G are connected to conductive “crowns” applied on the ends of the sample, so that the resistances of AB and FG “slices” can be measured in a 4-electrodes setting. Depending on the length of the sample, AB and FG “slices” may have slightly different thickness. In some experiments, the electrode between C and D was out of order, so the CD “slice” is twice as thick as the other ones.

CT-Scan Measurements

When a plateau is reached in the fluid production, the differential pressure and the electrical values, a CT scan is run. The CT-scanner used is a medical GE Fxi operated at 140 kV, 100 mA. One-millimetre thick slices are recorded every one millimetre. The image is reconstructed in a 512*512 matrix, thus providing a voxel $0.1*0.1*1 \text{ mm}^3$. About eighty images, from the inlet to the outlet of the cell are recorded. The “slices” in which the electrodes are included cannot be used, because of reconstruction artefacts related to the large X-ray absorption of the metal. So what can be interpreted is images in grey level of 6 or 7 1-mm thick slices between the electrodes. The average value of CT number and its standard deviation is computed over each slice and along the plug. Histograms of the grey levels of CT can also be calculated.

Choice of Fluids

In order to get a good contrast between the two fluids, oil and water, and the rock, a light oil, Soltrol 130 or Soltrol 170, is chosen. For the sandstones, a solution of $\text{BaCl}_2 \cdot 2\text{H}_2\text{O}$ 40 g/l is chosen. For experiments without CT-scan recording, NaCl solution has been used.

Choice of Rock Samples

In order to check the experimental design, the samples chosen to begin the program are Fontainebleau sandstones. These have already been studied by numerous authors since Jacquin [23] and are known as monomineral quartz and very homogeneous, since a porosity/permeability law can be drawn with confidence.

Porosity and Saturation Calculation

Bulk values of porosity and saturation are obtained from classical volume measurements. For local measurements, porosity and saturation are calculated as in many papers, by recording the CT values of the slices in several “pole” states, i.e. fully dry, fully saturated in brine and fully saturated in oil. Afterwards, a simple interpolation allows to estimate the porosity, or the saturation in one fluid. This procedure relies on many assumptions, among whose two are most important:

- in the range of energy (kVp and mA) used for the incident beam and in the range of composition of the solid and fluids in the samples, CT number is linearly proportional to saturation: that has been discussed in many papers;
- the “pole” states are real ones, i.e. exactly the same amount of air, of brine and of oil can be introduced in the same places of the rock. This may be verified, inasmuch as wettability is neglected, but may be difficult to achieve in case of microporosity.

The reason to assume these hypotheses is that it is quite difficult to calculate the absorption related to the physical environment (the cell, the confining fluid, the sleeve, the wires and electrodes used for the electrical measurements, the rock and the fluids) for all the voxels in the pore volume, given the fact that each voxel receives a different energy and is made of different stuff.

Experimental Procedures

A first step of characterisation is to get SEM images and Hg-injection curves that provide information on the porosity distribution, to be able to forecast the levels of pressure needed in the further experiments to change one fluid to another. A CT-scan of the plug outside the cell is recorded, showing the homogeneity or heterogeneity of this porosity distribution along the sample. Measurements of nitrogen and brine permeabilities follow, with at the same time, a CT scan of “dry” and “brine-saturated” sample in the cell, where the recorded signal undergo absorption due to the environment. These measurements are compared to the “dry, nude” images. Calculation provides the local values of porosity. Measurements of formation factor on each slice of the plug provide a local value of the formation factor, and, together with the porosity derived from the CT-scan, the local values of “m.” Simultaneous injection of oil and brine is begun, and the evolution of resistances, differential pressure and volumes is recorded. When a plateau is reached for the three measurements, a CT-scan is recorded, and the value of the fractional flow is changed.

RESULTS

Preliminary Characterisation

The Fontainebleau samples chosen have the K-phi values given in Table 1.

Table 1: Porosity(Hg) and permeability(brine) values of the Fontainebleau samples

Reference	Porosity (% PV)	Permeability mD
F21	21.0	280
F1.4	24.8	2200
F200	12.8	400

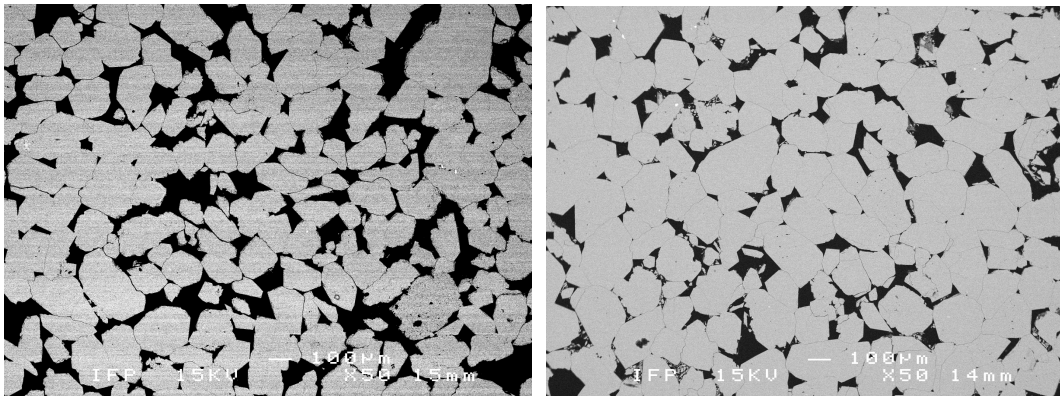


Figure 3: SEM images showing the porosity distribution.
(left): F1.4, (right):F200

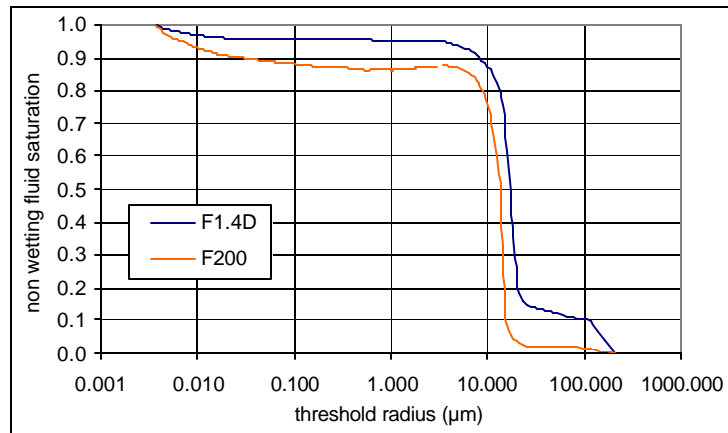


Figure 4: Pore threshold distribution drawn from mercury injection.

The distribution of pores and pore threshold can be drawn from the Scanning Electron Microscopy images (Figure 3) and the mercury injection (Figure 4). They show that the size of the pores is larger than 100 μm for the most porous sample, but the threshold is only about 16 μm ; however, about 10 % of the porous volume can be reached through thresholds larger than 100 μm . In the less porous, the number of large pores is lesser, and the threshold about 12 μm ; about 10 % of the porous volume can be reached by pore thresholds smaller than 0.01 μm . In both cases, more than 80 % of the porous volume can be reached with a capillary pressure of 1 bar in the mercury-vapour system.

Homogeneity of the Samples

CT values of the samples are calculated over the 1mm-slices, i.e. over about 80000 voxels, which in most cases encompass rock and porous volume, filled with any fluids. The results are given Table 2, for the dry samples.

Table 2: CT values average (1) and standard deviation (2) along the plug, (3) average of the standard deviation for each mm slice; porosity (1') calculated for the dry, nude plug, from calibration curves, and associated standard deviations, (2') and (3')

F21	(1) 1338	(3) 48	(1') 21.1 %	(3') 1.6 %
	(2) 16		(2') 0.5 %	
F1.4	(1) 1353	(3) 42	(1') 20.5 %	(3') 1.4 %
	(2) 10		(2') 0.3 %	
F200	(1) 1595	(3) 46	(1') 12.4 %	(3') 1.4 %
	(2) 11		(2') 0.1 %	

Standard deviations are calculated for each slice, and along the sample. Use of standard deviation assumes that the distribution is gaussian, which can be the case when the grains and pores are smaller than the voxel, i.e. each voxel encompass both solid and pores, and their size is rather homogeneous, which is checked on the SEM images. It appears clearly

on the chosen samples that the standard deviation along the plug is rather small, less than 0.5 %-PV, while within a slice it is higher, about 1.5 %-PV, due to the effect of partial volume of rock and pores in the voxels. Such figures allow a classification of rocks.

Formation Factor

Calculations of formation factor values have been performed on each slice, either with one salinity, or with several salinities. Continuous monitoring of the resistances show that the change in salinity is quite fast in these sandstones. Calculation of the “m” exponent of Archie has been performed with $a=1$, and the values of porosity drawn from the CT-scan.

Even on samples which are homogeneous, as shown by the porosity measurements, the value of the formation factor, thus of the “m” exponent, is somewhat higher when the measurement is taken at each end of the plug rather than in the inner parts.

Another point to emphasise is the range of values, between 1.5 and 1.8, for the “m” exponent, lower than the usually expected 2 value.

Table 3: Local measurements of Porosity, Formation Factor, and “m” calculation along the plugs compared to “bulk” values in bold font

F -21	AB	BC	CD	DE	EF		BE	AG
Local porosity (CT-scan)		0.226	0.205	0.205	0.210		0.212	0.212
Local Formation Factor		9.7	11.4	11.4	11.1		10.9	11.3
m (Archie, with $a=1$)		1.53	1.54	1.54	1.54		1.54	1.56
F1.4	AB	BC	CE		EF		BE	AG
Local porosity (CT-scan)	0.198	0.207	0.209		0.208		0.208	0.206
Local Formation Factor		12.2	11.4				11.7	13.3
m (Archie, with $a=1$)		1.59	1.55				1.56	1.64
F200	AB	BC	CD	DE	EF	FG	BF	AG
Local porosity (CT-scan)	0.129	0.126	0.124	0.120	0.120	0.117	0.123	0.122
Local Formation Factor	43.1	30.3	34.4	39.3	42.7	61.4	37.2	39.5
m (Archie, with $a=1$)	1.84	1.65	1.69	1.73	1.77	1.92	1.72	1.75

Resistivity Index

The first experiment performed on the F21 sample showed that end effects were non negligible, as recorded from the resistivity measurements alone, as seen on Figure 5. At the beginning of the first injection step of oil and brine simultaneously, there is a high resistivity on AB slice, which influences the measure of the total length resistivity on AG. This is interpreted as some accumulation of oil at the inlet. This first step shows as well the progressive invasion of oil in slices BC, CD and followings. On the following steps, this order is not so clear: it appears that the first oil invasion has to create a path that is used afterwards for floods with larger flow rates, inducing larger oil saturation. At the end of the drainage, the “slice” FG shows also high resistivity values, that may be related to an increase in the total flow rate, designed to reach lower S_w , leading to an oil accumulation.

As a consequence, RI vs Sw values for AB cannot be considered as representative; for FG they can for the low flow rates, but cannot for the high flow rates, and consequently AG values, taken at the two ends, are not correct. So, in this case, taking the values on BF appears as a good compromise, but examination by CT-scan of the real location of the fluids seems very attractive.

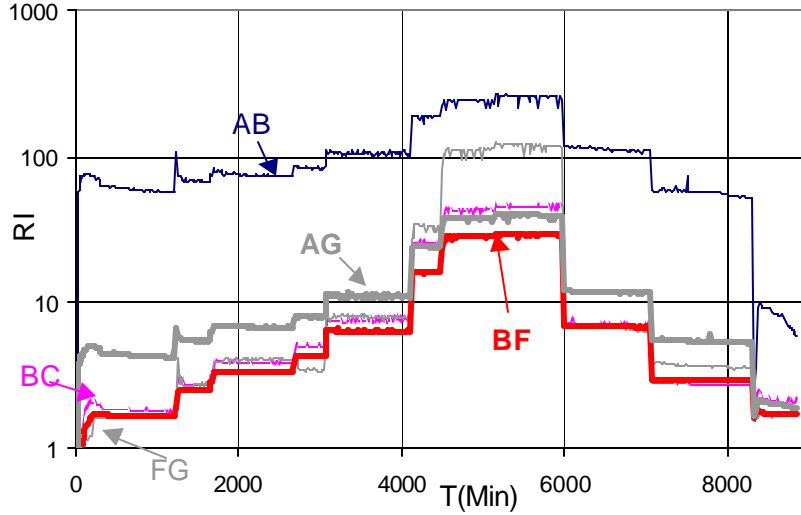


Figure 5: Resistivity index recorded on different “slices” of the F21 plug, during drainage and imbibition.

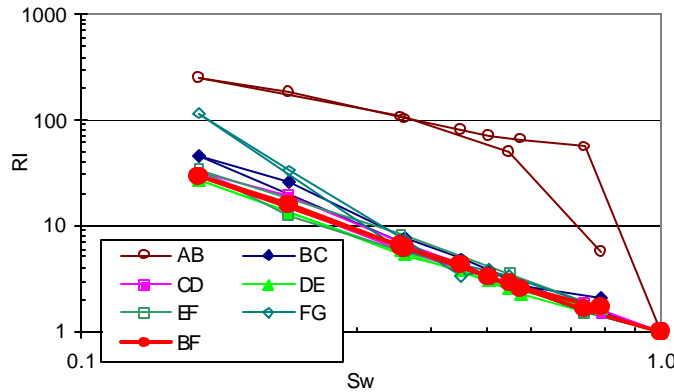


Figure 6: Relationship between RI and Sw, for different slices of the F21 plug, showing artefacts on AB and FG.

Subsequent experimentations including CT scan have thus been designed, and results are shown on Figure 7. Interpretation is made from careful examination of the images, and average CT calculations.

Sample F1.4, which is very permeable, could not be processed with a sufficient differential pressure to overcome the end effect due to capillary pressure: as the drainage proceeds,

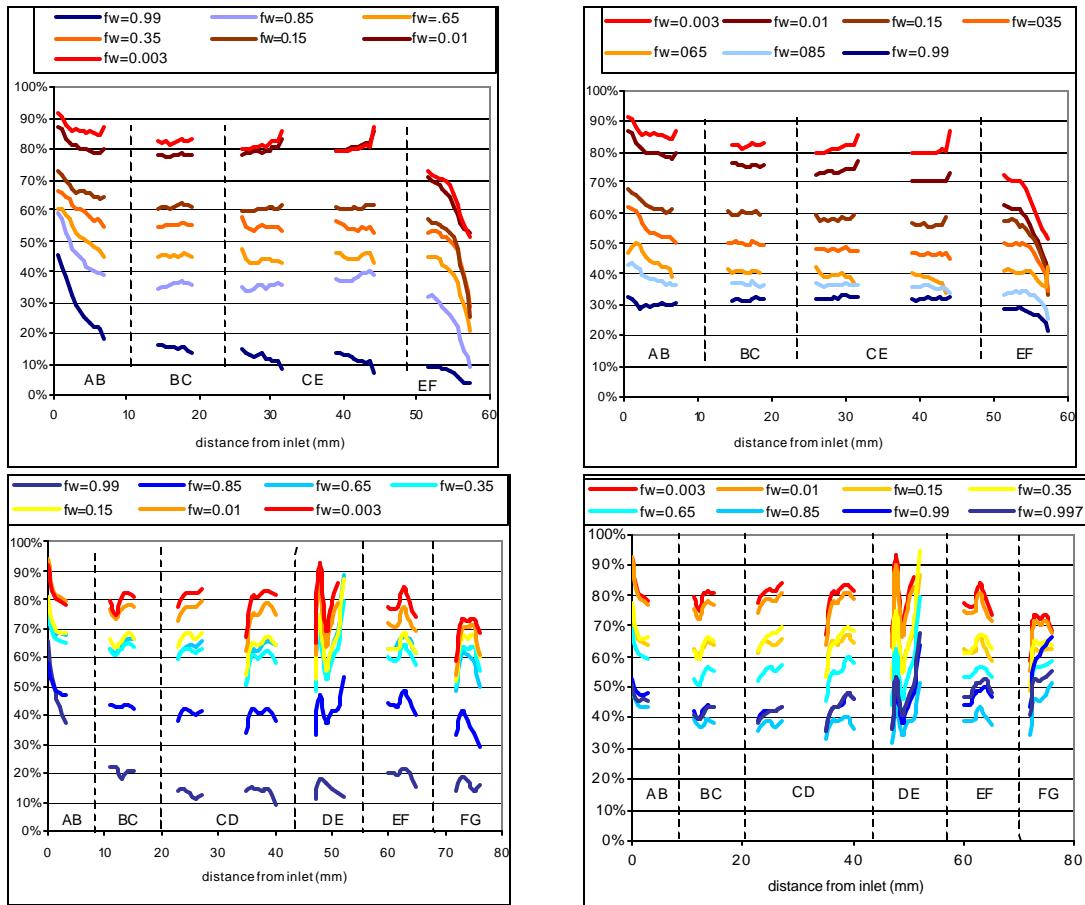


Figure 7: Local oil saturation from CT scan for F1.4 (high permeability, higher figures) and F200 (low permeability, lower figures).during steady state oil brine tests in drainage (left) and imbibition (right)

Table 4: Local “n” values for the Fontainebleau sandstones compared to “bulk” values in bold font

F21		BC	CD	DE	EF		BF	AG
n		2.04	1.87	1.72	1.83		1.83	2.28
R ²		0.98	0.99	0.99	0.98		1.00	0.94
F1.4	AB	BC	CE	EF			BE	AG
n	2.33	2.07	1.87	3.74			1.97	2.38
R ²	0.97	0.99	0.97	0.98			0.98	1.00
F200	AB	BC	CD	DE	EF	FG	BF	AG
n	1.96	2.21	2.02	1.38	2.55	2.86	2.08	2.19
R ²	0.97	0.99	1.00	0.99	0.96	0.90	0.98	0.99

water saturation remains high in the last slices, about 5 mm from the outlet. During the same time, the resistance values increase, probably due to oil accumulation at the outlet, outside the plug. At the inlet, oil accumulation is high from the first step, and remains higher than in the middle of the sample during the whole experiment.

Sample F200, which is less permeable, shows the same behaviour at the inlet, along a few millimetres; the capillary foot at the outlet is quite negligible, but the resistances are however high. The most homogeneous distribution of the fluids is found also in the middle of the sample.

Calculation of the “n” saturation exponent value can thus be done with more significance in the parts of the sample where the distribution is actually homogeneous. Results are given in Table 4. They show that discarding of the two ends, inlet and outlet, and calculation over the middle slices give “n” values which are lower by up to 0.4 in permeable samples than those drawn directly from end measurements. The results are close to the usually expected 2 value.

DISCUSSION

The “steady state” procedure has been recommended as a way to put the fluids in place in a homogeneous distribution in order to measure significant resistivity index. However, it can be considered a rather long process, that is why numerous works have used other designs to put the fluids in place. It appears from the present work that, at least for reasonably permeable samples, with no microporosity, a full drainage-imbibition cycle can be performed in about 6 to 10 days.

Depending on the permeability of the samples, and on the flow rates used, capillary foot effect can induce errors in the calculation of the RI, which are not healed by using a “bump” procedure. Use of a “bump, or significant increase in flow rate in an effort to lower residual saturation is frequently used, to get additional values for relative permeabilities as well. It appears from the present experiments that the distribution of fluids is then no longer homogeneous along the core, thus that the flow phenomena are not comparable. In any case, resistivity indexes cannot be calculated from such states with the aim of using them for log interpretation.

CT scan control of the distribution of fluids allow reasonable choice of homogeneous states to make an interpretation, at least for resistivity indexes.

CONCLUSION

Most interpretations of fluid flow in reservoir engineering rely on assumptions of homogeneous samples and homogeneous fluid distribution. In actual samples these assumptions may not be fulfilled.

On the other hand, experimental artefacts, e.g. related to the sample size and the flood experimental conditions, can lead to erroneous interpretation that may induce large errors

in formation factor and resistivity index estimations and large consequences when extrapolating to larger scales.

Description of the distribution of saturation by quantitative interpretation of CT-scan measurements at the millimetre scale helps explaining how the fluids flow and reach or not stationary states, and allow discarding of the zones disturbed by artefacts. Local continuous measurements of resistivity index along the core can be related to the distribution of saturation. Comparing both information help designing experiments with a clearer knowledge of the phenomena taking place.

Sound RI-Sw relationships obtained in clearly defined states can be used better than rough ones for extrapolation at higher scales.

ACKNOWLEDGMENTS

This work benefited from skills of C. Lemaire, B. Pigeat and S. Landais for the flow experiments, C. Fichen and C. Schlitter for the CT-scan, E. Rosenberg for the SEM, and J.M. Nez for the mercury injection..

NOMENCLATURE

K: permeability (mDarcy)

F: formation factor, defined as

$$F = \frac{R_o}{R_w}$$

RI : resistivity index, defined as

$$RI = \frac{R_t}{R_o}$$

R_w the resistivity of brine,

R₀ the resistivity of rock at S_w= 100 %,

R_t the formation resistivity

m, Archie cementation factor, defined as:

$$F = \frac{a}{\Phi^{-m}},$$

Φ: the porosity (volume fraction)

a: “tortuosity” parameter, usually comprised between 0.6 and 1

n, Archie saturation exponent, defined as:

$$RI = S_w^{-n}$$

CT : Hounsfield unit, defined as :

$$CT_{object} = \frac{\mu_{object}^? - \mu_w^?}{\mu_w^?} * 1000$$

μ mass attenuation coefficient (cm²/g),

ρ volume mass of the material (g/cm³),

object and w (for water)

So and Sw: saturations in oil and water

REFERENCES

- 1 Archie, G.E. “The electrical resistivity log as an aid in determining some reservoir characteristics.” *Petroleum Transactions, AIME*, (1942) v. 146, pp 54-62.
- 2 Wellington, S.L. and Vinegar, H.J. “X-ray Computerized Tomography” SPE paper 16983, *Journal of Petroleum Technology*, (August 1987), pp 885-898.
- 3 Withjack, E.M. “Computed Tomography for Rock-Property Determination and Fluid-Flow Visualization”. *SPEFE*, Dec. 1988 pp 696-704 (Revised SPE 16951)
- 4 Withjack, E.M., Graham, S.K. and Yang, C.T. “CT Determination of Heterogeneities and Miscible Displacement Characteristics” *SPEFE*, Dec. 1991 pp 447-452 (Revised SPE 20490).
- 5 Rust, C.F. “Electrical resistivity measurements on reservoir rock samples by the two-electrode and four-electrode methods.” *Petroleum Transactions, AIME*, (1952)v. 195, pp 217-224.
- 6 Lewis, M.G., Sharma, M.M., Dunlap, H.F. and Dorfman, M.H. “Techniques for measuring the electrical properties of sandstone cores.” SPE 18178, 63th ATCE, Houston, Oct. 2-5, 1988.

- 7 Sprunt, E.S., Hensel, W.M., Jr., York, C.E., and Honarpour, M.M. "Compilation of electrical resistivity measurements as performed by twenty-five laboratories." *The Log Analyst*, (1988) v 29, no 1, pp 13-39.
- 8 Worthington, A.E., Hedges, J.H., Pallatt, N. "SCA guidelines for sample preparation and porosity measurement of electrical resistivity samples. Part I: Guidelines for preparation of brine and determination of brine resistivity for use in electrical resistivity measurements." *The Log Analyst*, Jan-Feb. 1990, pp 20-28.
- 9 Lerner, D.B., Dacy, J.M., Raible, C.J., Rathmell, J.J., Swanson, G. and Walls, J.D. "SCA guidelines for sample preparation and porosity measurement of electrical resistivity samples. Part II: Sample preparation and porosity measurement." *The Log Analyst*, Mar-Apr 1990, pp 57-63.
- 10 Worthington, P.F., Evans, R.J., Klein, J.D., Walls, J.D., and White, G. "SCA guidelines for sample preparation and porosity measurement of electrical resistivity samples. Part III — The mechanics of electrical resistivity measurements on rock samples." *The Log Analyst*, March-April 1990, pp 64-67.
- 11 Maerefat, N.L., Baldwin, B.A., Chaves, A.A., LaTorraca, G.A., and Swanson, B.F. "SCA guidelines for sample preparation and porosity measurement of electrical resistivity samples Part IV: Guidelines for saturating and desaturating core plugs during electrical resistivity measurements." *The Log Analyst*, March-April 1990, pp 68-74.
- 12 Lyle W.D. and Mills, W.R. "Effect of Nonuniform Core Saturation on Laboratory Determination of the Archie Saturation Exponent" *SPEFE*, March 1989, pp 49-52 (Revised SPE 17143)
- 13 Sprunt, E.S., Desai, K.P., Coles, M.E., Davis, R.M., Muegge, E.L. "CT-Scan-Monitored Electrical Resistivity Measurements Show Problems Achieving Homogeneous Saturation." SPE 21433 (ATCE 1991).
- 14 Baldwin, B.A. and Yamanashi, W.S. "Persistence of Non uniform Brine Saturation Distribution in CSA Electrical Resistivity Study Core Plugs after Desaturation by Centrifuging." *The Log Analyst*, Jan-Feb 1989, pp 45-48
- 15 De Waal, J.A., Smits, R.M.M., De Graaf, J.D. and Schipper, B.A. "Measurements and evaluation of resistivity-index curves" *The Log Analyst*, Sept-Oct 1991, pp 583-595.
- 16 Jing, X.D., Gillespie, A. and Trewin, B.M. "Resistivity index from Non-Equilibrium Measurements Using Detailed In-Situ Saturation Monitoring". SPE 26798 (ATCE 1993).
- 17 Gray, R. Trewin, B., Pallatt, N., and Mitchell P. "Comparison of Saturation Exponent Data by the "Porous Plate" and by the "Continuous Injection" Technique with In-Situ Saturation Monitoring." *3rd SCA Symp. Proc.* (1993) pp 203-313.
- 18 Coenen J.C.C. and Koorneef " State-of-the-art X-ray Steady State Apparatus for advanced core flow studies" SCA-9853, 1998, The Hague.
- 19 Chambre syndicale de la Recherche et de la Production du Pétrole et du gaz naturel. "Recommandations pour la détermination des profils de porosité et de saturation dans les milieux poreux par absorption d'un rayonnement X." *Revue IFP*, vol 41, n°3, May-June 1986.
- 20 Maloney D., Wegener D., Zornes D. "New X-Ray Scanning System For Special Core Analyses In Support Of Reservoir Characterization" SCA-9940, 1999, Denver, pp 395-404.
- 21 Maloney, D., Wegener, D.C., Zornes, D.R. "Significance of Absorption Coefficients When Determining In situ Core Saturation by Linear X-ray Scans" SCA 2000-13, 2000, Abu Dhabi.
- 22 Durand, C. " Combined Use of X-ray CT Scan and Local Resistivity Measurements: A New Approach to Fluid Distribution Description in Cores." SPE 84299, to be presented at the ATCE, 2003.
- 23 Jacquin, C. "Corrélations entre la perméabilité et les caractéristiques géométriques du grès de Fontainebleau." *Rev. I.F.P.*(1964) XIX, 7-8, pp 921-937.